Simulation of HF Ground Backscatter Measured by the Ekaterinburg SuperDARN Radar. Comparison with Observations

A. V. Oinats, K. A. Kutelev, and V. I. Kurkin
Institute of Solar-Terrestrial Physics SB RAS, Russia

Abstract— We study diurnal-seasonal pattern of HF ground backscatter characteristics such as minimum slant range, corresponding elevation angle, true reflection height etc.. All characteristics are calculated taking into account the Ekaterinburg SuperDARN HF radar (Ekb; 56.4°N, 58.5°E) technical specifications. We use original technique for HF simulation based on waveguide approach as well as ray tracing technique and international reference ionosphere (IRI-2012) as a propagation media. We compare simulation results with the Ekb data recorded during 2013–2014 and estimate an accuracy of IRI-2012 prediction. Current study might be useful for IRI model testing in the sub-polar region and for further improvement of Ekb data interpretation.

1. INTRODUCTION

The Ekaterinburg SuperDARN High Frequency (HF) radar [1] (Ekb; 56.4°N, 58.5°E) measures the echoes from the ranges of about 180 km to 3500 km. The Ekb antenna system represents a phased array which allows to form a narrow radiation pattern (azimuthal width of ∼3.24°), called "beam", in the 16th azimuthal directions. The radar field-of-view width is about 50° with a boresite azimuth of 20° (clockwise from North). Radar scans sequentially all 16 beams in the standard operation mode. Duration of the whole scan is about 2 min. There are two types of echo in radar data: ionospheric scatter and ground backscatter (GB). Ionospheric scatter is typically irregular, because it is caused by HF wave reflection by geomagnetic field-aligned plasma inhomogeneities of decameter scale. GB is caused by HF wave scattering by ground surface roughness. Its behavior is mostly determined by regular change (diurnal and seasonal) of the ionosphere and, therefore it is more predictable than ionospheric scatter.

In the paper, we present simulated diurnal and seasonal behavior of the main HF GB characteristics corresponding to skip distance, such as minimum slant range, elevation angle and true ionospheric reflection height. We use original HF calculation techniques and global reference ionosphere model IRI-2012 [2]. We discuss the features of the characteristics and compare them with observational ones recorded by the Ekb radar from 2007 to 2014. We evaluate the IRI-2012 accuracy during different seasons, local time and for different directions of HF sounding traces in the sub-polar region.

2. TECHNIQUE FOR HF GROUND BACKSCATTER SIMULATION

Technique for HF GB simulation [3, 4] is based on adiabatic approach of eigenfunction method [5]. In case of azimuthally symmetric Earth-ionosphere waveguide electromagnetic field induced by arbitrary emitter is expressed by a series of eigenfunctions as,

$$E\left(\vec{r},t\right)\sim \mathrm{Re}\left\{\sum_{n} I_n\left(\varphi\right) A_n\left(\vec{r}\right) g_0\left(t-\tau_n(\vec{r})\right) e^{i\Phi_n(\vec{r})-i\omega_0 t}\right\}. \quad (1)$$

In Expression (1) we use spherical coordinate system with origin in the Earth's center, $\tau_n(\vec{r})$, $A_n(\vec{r})$ and $\Phi_n(\vec{r})$ are the time lag, amplitude and phase of eigenfunction with number n respectively, $g_0(t)$ is envelope of the transmitted signal, $I_n(\varphi)$ is an excitation coefficient, which is determined by characteristics of emitter or scattering features of rough ground surface [3, 4], ω_0 is a cycle frequency. We do not place here the full expressions for time lag, amplitude and phase of eigenfunction because of their bulkiness.

Expression (1) represents the spatial-temporal distribution of the HF amplitude inside the waveguide. The summing in (1) is carried out for all eigenfunctions that are effectively "exited" by the emitter and weakly "penetrate" through the ionosphere. Such a set consists of several thousand of eigenfunctions in case of the F2 ionospheric HF channel. Technique, that is more effective, operates with stationary condition, which describes the interference features of eigenfunction series as,

$$L_n^{\pm}\left(\vec{r},f\right)=\frac{1}{2\pi}\left(\Phi_n^{\pm}(\vec{r})-\Phi_{n+1}^{\pm}\left(\vec{r}\right)\right)=l^{\pm}. \quad (2)$$

Here f is an operating frequency, $l^{\pm}$ is a hop number. Expression (2) defines the phased eigenfunction set and allows us to determine the HF propagation modes and their characteristics. We also used another technique that is based on ray tracing approach. Comparison showed that calculation results obtained by two different techniques are in a good agreement. Therefore, further we present the results obtained using the technique described above.

3. CALCULATION RESULTS

Figure 1(a)–Figure 1(f) show regular diurnal and seasonal dependencies of minimum slant range (Figure 1(a), Figure 1(d), and Figure 1(g)), elevation angle (Figure 1(b), Figure 1(e), and Figure 1(h)) and true reflection height (Figure 1(c), Figure 1(f), and Figure 1(i)) for E and F2 ionospheric HF channels respectively. The dependencies are calculated for beam #0 of the Ekb radar (azimuth of 4.3° counterclockwise from North) for period from 2013 to 2014. Operating frequency is 11 MHz. Separation of the echoes propagating in two HF channels (E and F2) is performed by checking the true reflection height value. Figure 1(g), Figure 1(h), and Figure 1(i) present the dependencies of E and F2 layer critical frequency (Figure 1(a), Figure 1(b), Figure 1(d), Figure 1(e), Figure 1(g), and Figure 1(h)) and F2 layer maximum height (Figure 1(c), Figure 1(f), and Figure 1(i)) for electron density profile at the reflection point. The characteristics are calculated for 15-th day of each month with 1-hour step in local time. IRI "storm" option is turned off. As we can see from Figure 1(a)–Figure 1(f), there are local time intervals when regular GB is completely absent. For E channel GB is absent in winter at all and during nighttime in summer and equinox. For F2 channel GB is absent during winter nighttime. This is well explained by low critical frequency during these local time intervals (see Figure 1(g) and Figure 1(h)) when HF waves totally pass through the ionosphere without reflection.

Diurnal minimum of slant range in E channel is located near the noon (see Figure 1(a)) when crit-

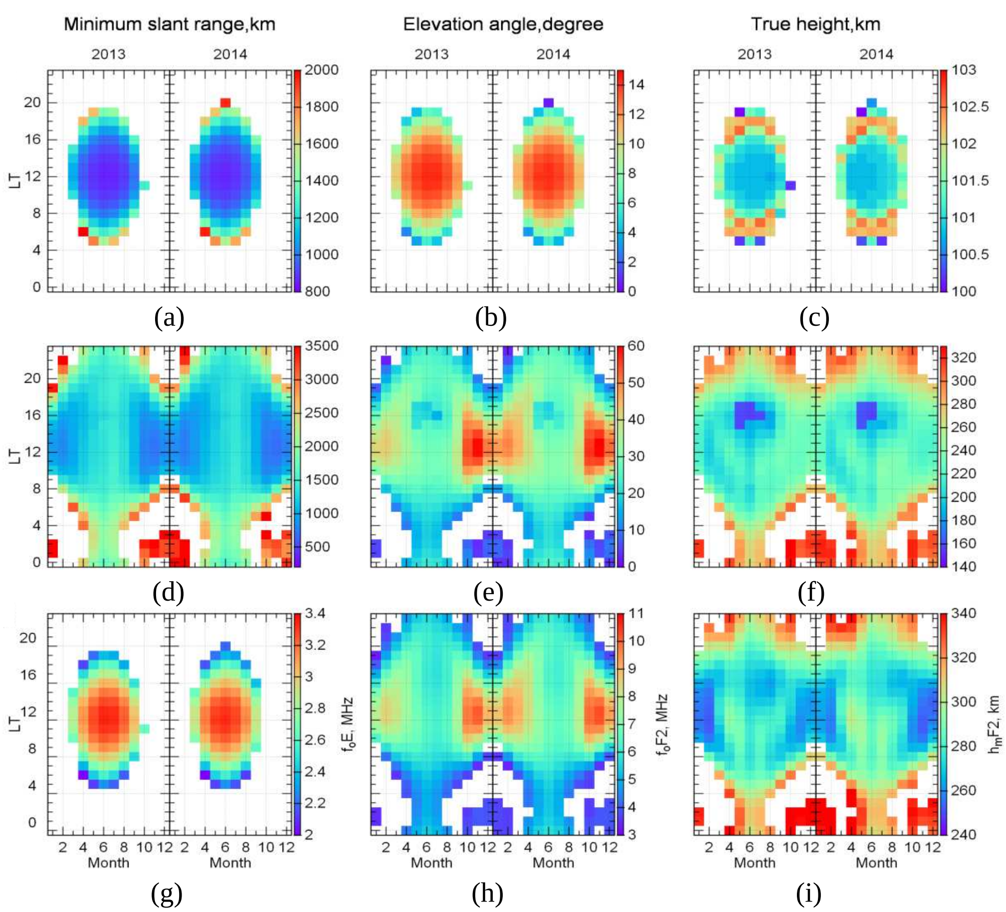

Figure 1: Simulated minimum slant range, corresponding elevation angle and true height for (a), (b), (c) E-channel and (d), (e), (f) F2-channel. (g), (h), (i) Critical frequency of E and F2 layers and maximum height of F2 layer.

ical frequency has its maximum. Increasing/decreasing critical frequency causes decrease/increase of minimum slant range during morning/evening hours. Slant range in F2 channel has similar behavior in winter and equinox (see Figure 1(d)). However, decrease of F2 layer critical frequency is often accompanied by increase of the maximum height (and vice versa). Therefore, the slant range varies more rapidly in F2 channel than in E channel. There are two local maximums of slant range diurnal dependence in summer at noon and mid-night. Comparing the plots for 2013 and 2014, we can see that minimum slant range decreases in general when solar activity increases. Diurnal and seasonal dependence of skip distance repeats in detail the minimum slant range behavior with difference only in absolute values. The deviation between minimum slant range and skip distance varies in the following ranges: ∼20–40 km in E channel, and ∼100–300 km in F2 channel.

The dependence of elevation angle (see Figure 1(b) and Figure 1(e)) repeats the behavior of critical frequency. The higher the critical frequency the higher the elevation angle. Simple relation between plasma frequency in the reflection point and elevation angle can be derived from generalized Snell's law [6]. Measurement of elevation angle makes it possible to estimate the critical frequency with accuracy up to 10% for distances up to 2000 km from radar. Unfortunately, the Ekb radar is currently unable to measure elevation angle.

Behavior of the true reflection height (see Figure 1(f)) in F2 channel is determined mostly by change of maximum height (see Figure 1(i)). The true reflection height is lower than corresponding maximum height approximately by 40 km. HF radar does not measure true reflection height. Instead, we can estimate an effective reflection height using measured slant range and elevation angle. Effective reflection height varies in a wide range from about 200 to 500 km in F2 channel and from 115 to 130 km in E channel. Thus using the effective height it would be possible to separate E echoes from F2 echoes. The correct estimate of the effective height is also important for mapping of the HF radar echoes. Researches often use fixed effective height value that leads to a systematic error up to 250 km for F2 channel. Elevation angle measurements provide reduction of the error in twice or even more.

In case of GB mapping, regular ionospheric gradients lead to systematic error up to about 100 km. Estimation of the ratio between full slant range to the ground and slant range to the reflection point shows that regular ionospheric gradients are mainly negative along all beams of Ekb radar. This is because all beams are oriented northwards. The ratio for beam #0 is about 2.1 on average, but for some local time interval can reach values of ∼2.3. Using simulated characteristics described above, it is possible to take into account this effect.

4. COMPARISON WITH OBSERVATIONS

We processed the entire Ekb radar dataset from 2013 to 2014 using a technique for automated extraction of the minimum slant range from SuperDARN radar data [7]. HF characteristics described above were used for reliable identification of the echoes related to the one-hop F2 channel regular GB. After extraction, we averaged obtained time dependencies near the integer local time values (±0.15 h) over all geomagnetic quiet days ($Kp < 3$) of certain month. Figure 2 shows diurnal and seasonal variations of the calculated monthly mean minimum slant range for beam #0. Comparing with Figure 1(d), one can see that in general behavior of the observed slant range agree with simulated one. The main difference is concerned with summer diurnal behavior. The local maximums in the observed diurnal dependence occur in the morning and evening, instead of noon and mid-night as seen from simulated pattern (see Figure 1(d)). Simulated values are greater than observed ones by ∼200–300 km on average. The greatest deviation is seen in late spring and summer months. Maximum observed monthly mean slant range does not exceed ∼2600 km, but maximum simulated slant range reaches ∼3800 km. The overestimation of the minimum slant range on average most probably can be associated with systematic underestimation of the critical frequency by IRI-2012 model within the Ekb field-of-view.

Figure 3 represents a scatter plot of the observed monthly mean slant range versus simulated one. There is a distinct effect of saturation for observed slant range in its low and high part. The low threshold is about ∼700 km. The high threshold is about ∼2500 km. The observed saturation most likely can be related with peculiarities of the Ekb antenna system which limits the lowest and highest elevation angle with some threshold.

Figure 4 shows the relative yearly mean difference between simulated and observed slant range for all 16 beams and for 2013 and 2014 separately. As we can see the maximum difference is about 32% obtained for beam #11 in 2013, the minimum difference is equal to 18% for beam #8 in 2014. There is no distinct dependence on beam number. However, there is a distinct dependence on the

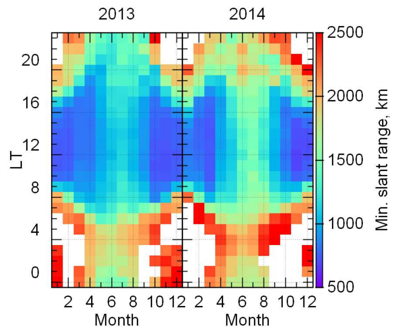

Figure 2: Observed monthly mean slant range.

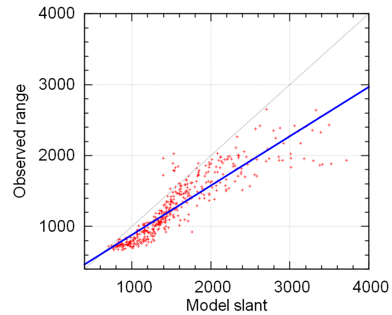

Figure 3: Regression between observed and simulated slant range.

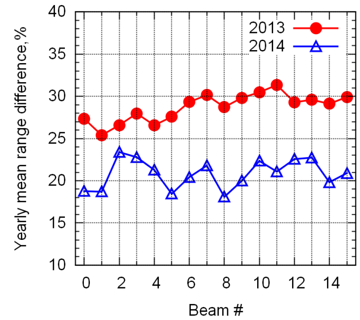

Figure 4: Yearly mean difference dependence on the beam number.

solar activity level: the difference is lower for year of higher solar activity.

5. CONCLUSIONS

We presented the GB simulation results related to the Ekaterinburg SuperDARN HF radar from 2013 to 2014. The simulation was performed using the original technique based on waveguide approach and global ionosphere model IRI-2012. We studied diurnal and seasonal behavior of minimum slant range, elevation angle and true reflection height corresponding to HF skip distance. All these characteristics have distinct diurnal and seasonal pattern, which can be qualitatively explained by regular change of the critical frequency and maximum height of corresponding ionospheric layers in the point of HF wave reflection. We studied the systematic error of standard SuperDARN mapping technique. Application of fixed effective reflection height leads to distance deviation up to 250 km. However, elevation angle measurements could noticeably improve the accuracy of mapping. In addition, elevation angles might be used for separation of the echoes, propagating in different HF channels, and for estimation of ionospheric critical frequency.

Simulated slant ranges agree with observed monthly mean qualitatively. However, simulated values are greater than observed ones by ∼200–300 km on average. This most probably can be associated with systematic underestimation of the critical frequency by IRI-2012 model within the Ekb field-of-view. We also found distinct effect of saturation for the observed slant range, which most likely can be related with peculiarities of the Ekb antenna system. The yearly mean difference between simulated and observed slant range varies from 18% to 32% depending on beam number and year. It is lower for year of high solar activity.

ACKNOWLEDGMENT

This work was done under financial support of Russian Foundation for Basic Research (grants No. 14-05-00259).

REFERENCES

1. Chisham, G., M. Lester, S. E. Milan, M. P. Freeman, W. A. Bristow, A. Grocott, K. A. McWilliams, J. M. Ruohoniemi, T. K. Yeoman, P. L. Dyson, R. A. Greenwald, T. Kikuchi, M. Pinnock, J. P. S. Rash, N. Sato, G. J. Sofko, J.-P. Villain, and A. D. M. Walker, "A decade of the super dual auroral radar network (SuperDARN): Scientific achievements, new techniques and future directions," *Surv. Geophys.* Vol. 28, 33–109, 2007.
2. Bilitza, D., D. Altadill, Y. Zhang, C. Mertens, V. Truhlik, P. Richards, L.-A. McKinnell, and B. W. Reinisch, "The International Reference Ionosphere 2012 — A model of international collaboration," *J. Space. Weather. Space Clim.*, Vol. 4, No. A07, 1–12, 2014.
3. Ponomarchuk, S. N., V. I. Kurkin, and A. V.Oinats, "The diagnostics of ionosphere and earth ground surface by backscatter sounding data," *PIERS Proceedings*, 1307–1310, Moscow, Russia, Aug. 18–21, 2009.
4. Oinats, A. V., V. I. Kurkin, K. A. Kutelev, and N. Nishitani, "The outlook of SuperDARN radars application for monitoring of the ionospheric dynamics in Russia," *Physical Bases of Instrumentation*, Vol. 1, No. 3, 3–18, 2012 (in Russian).
5. Kurkin, V. I., I. I. Orlov, and V. N. Popov, *Normal Wave Technique in HF Radio Communication Problem*, Nauka, Moscow, 1981.

6. Davies, K., *Ionospheric Radio*, Peter Peregrinus Ltd., London, 1990.
7. Oinats, A. V., V. I. Kurkin, and N. Nishitani, "Statistical study of medium-scale traveling ionospheric disturbances using SuperDARN Hokkaido ground backscatter data for 2011," *Earth Planets Space*, Vol. 67, 22, 2015.